An underwater visual SLAM system with adaptive image enhancement

An underwater visual SLAM system with adaptive image enhancement

Gang Chen [a,b,c], Guoqiang Du [a], Chenguang Yang [d], Yidong Xu [a], Chuanyu Wu [e,a], Huosheng Hu [f], Fei Dong [g], Jinfeng Zeng [a,h]

[a] School of Mechanical Engineering, Zhejiang Sci-Tech University, Hangzhou 310018, China
[b] Zhejiang Marine Intelligent Ship Institute, Hangzhou 310015, China
[c] Donghai Laboratory, Zhoushan 316021, China
[d] Department of Computer Science, University of Liverpool, Liverpool, L69 3BX, UK
[e] Zhejiang Ocean University, Zhoushan 316022, China
[f] School of Computer Science and Electronic Engineering, University of Essex, Colchester CO4 3SQ, UK
[g] Zhejiang Chengshi Robot Co., Ltd., Jiaxing 314203, China
[h] Hangzhou Hanlu Subsea Technology Co., Ltd., Hangzhou 311202, China

ARTICLE INFO

Keywords:
Adaptive image enhancement
Serial-parallel fusion processing strategy
Simultaneous localization and mapping
Underwater environment recognition
Underwater monocular vision

ABSTRACT

Underwater monocular visual simultaneous localization and mapping (SLAM) plays a crucial role in the navigation and localization of underwater robots. Low-light and turbid underwater environments pose significant challenges to the effectiveness and accuracy of these systems. This paper proposes a novel recognition algorithm based on the AquaVisNet model, designed specifically for such environments. Furthermore, an image enhancement algorithm tailored for these challenging environments is proposed that utilizes a serial-parallel fusion processing strategy. Such enhancement improves image quality significantly. Building on these advancements, an adaptive image enhancement ORB-SLAM (AIE-ORB-SLAM) system is presented for low-light and turbid underwater environments. The experimental results demonstrate that this system significantly outperforms the ORB-SLAM3 system in terms of various metrics. Under low-light, turbid, and combined conditions, the AIE-ORB-SLAM system improves the initialization time by 23.46%, 23.88%, and 81.69%, respectively; the tracking duration by 72.63%, 235.12%, and 294.29%, respectively; the number of keyframes by 74.71%, 140.00%, and 218.48%, respectively; the number of point clouds by 119.19%, 187.92%, and 317.11%, respectively; and the localization accuracy by 90.04%, 75.61%, and 66.81%, respectively. These results demonstrate that the proposed method significantly enhances the robustness and localization accuracy of underwater visual SLAM systems in low-light and turbid environments.

1. Introduction

With the widespread use of underwater robots in the field of ecological detection of marine coral colonies (Zhang et al., 2022a), (Hu et al., 2021), (Chen et al., 2023), the investigation of simultaneous localization and mapping (SLAM) systems in underwater settings has gained significant attention. Underwater SLAM, as an automated navigation technique (Huang et al., 2020), does not rely on external data sources and solely utilizes sensor data to estimate attitudes and create environmental maps for autonomous underwater vehicles (AUVs) or remotely operated vehicles (ROVs). Additionally, the position of underwater robots can be autonomously determined based on an environmental map (Cheng et al., 2021), (Yan et al., 2024), (Chen et al., 2025a). Underwater SLAM can be classified into several types based on sensor technology, including light detection and LiDAR SLAM, sonar SLAM, and visual SLAM (Hess et al., 2016), (Mattern et al., 2021). Compared to other underwater SLAM sensors, underwater monocular visual SLAM offers the advantage of providing high-resolution underwater imagery and color information about objects in the aquatic environment. It also has the benefits of cost-effectiveness in sensing, simple structure, strong anti-interference ability, and low computational resource demand (Barros et al., 2022), (Hodne et al., 2022).

Unlike controlled terrestrial or indoor settings, underwater environments present unstructured characteristics and are susceptible to various forms of interference and noise (Wang et al., 2023), (Chen et al., 2024). These characteristics introduce numerous complexities and

challenges to underwater visual SLAM. Seawater, with its complex chemical composition and substantial presence of suspended matter and organic compounds (Zhang et al., 2022b, (Guo et al., 2020, leads to diminished image contrast due to light scattering and absorption. Furthermore, the nonuniformity of seawater results in significant image distortion (Li et al., 2020, (Xu et al., 2021, (Jang et al., 2021. Hidalgo et al. determined experimentally that monocular ORB-SLAM performs well in underwater settings characterized by adequate illumination, minimal flicker, and an abundance of scene features (Hidalgo et al., 2018. Joshi et al. conducted a comparative assessment of several visual SLAM algorithms for underwater sequences and revealed that the efficacy of visual SLAM systems is still adversely affected due to underwater image turbidity and low contrast (Joshi et al., 2019. The aforementioned literature examines the factors contributing to the diminished performance of monocular visual SLAM in underwater settings, including concerns such as image blurring, and reduced contrast. Further research and refinement are necessary to enhance the resilience and localization precision of underwater visual SLAM systems within underwater domains.

Xin et al. proposed an underwater monocular visual SLAM system specialized for underwater low-light environments. The system is based on the ORB-SLAM2 framework and incorporates underwater image enhancement techniques (Xin et al., 2023. Zheng et al. presented an underwater monocular visual SLAM system for underwater turbid environments, based on the ORB-SLAM3 framework. The results show that ORB-SLAM3 outperforms both ORB-SLAM2 and Dual-SLAM in complex underwater environments. Additionally, integrating underwater image enhancement techniques within the ORB-SLAM3 framework enhances the overall performance of the SLAM system (Zheng et al., 2023. Liu et al. developed an underwater monocular visual SLAM approach based on the Exposure Sub-Image Histogram Equalization image enhancement method within the ORB-SLAM3 framework. This approach enhances images thereby improving the pose estimation precision of the SLAM technique (Liu et al., 2023. Research indicates that ORB-SLAM3 performs exceptionally well in various environments and is widely adopted by scholars as a framework for underwater monocular visual SLAM, often combined with a single image enhancement algorithm to improve performance in low-light or turbid conditions. However, these methods lack an adaptive image processing strategy tailored to different underwater environmental conditions. When underwater conditions change, the underwater monocular visual SLAM relying solely on a single image enhancement technique struggles with degraded images, resulting in issues such as loss of tracking and incorrect localization. Consequently, enhancing the performance of underwater monocular visual SLAM in dynamically changing low-light and turbid underwater environments remains an unresolved challenge.

To address the issue of diminished performance in underwater monocular visual SLAM under dynamic low-light and turbid conditions, this study proposes an adaptive image-enhanced underwater visual SLAM system (AIE-ORB-SLAM).This system is specifically designed to operate effectively in challenging underwater environments. Building upon the ORB-SLAM3 framework, AIE-ORB-SLAM combines a recognition algorithm designed for low-light and turbid underwater conditions using the AquaVisNet model with an image enhancement algorithm that addresses the challenges of low-light and turbid underwater conditions through a serial-parallel fusion processing strategy. The noteworthy innovations in this paper include the following:

(1) The proposed underwater visual SLAM system, which features adaptive image enhancement for low-light and turbid underwater environments, effectively addresses the challenge of performance degradation faced by underwater visual SLAM under such conditions. This innovation enhances the robustness and accuracy of visual SLAM in dynamic underwater environments.
(2) A recognition algorithm for underwater low-light and turbid environments utilizing the AquaVisNet model is proposed. This algorithm accurately identifies the prevailing conditions in low-light and turbid underwater settings. Moreover, the algorithm undergoes training with images from the current underwater environment, ensuring its resilience and accuracy across diverse underwater scenarios.
(3) An image enhancement algorithm for underwater low-light and turbid conditions utilizing a serial-parallel fusion processing strategy is proposed. The algorithm effectively restores dynamic underwater images affected by low light and turbidity, improves image contrast, reduces image haziness, enhances texture information, and improves image feature point extraction and matching performance.

The subsequent sections of the paper are structured as follows: Section 2 outlines the architecture of an underwater visual SLAM system with adaptive image enhancement. Section 3 explains the model structure of the recognition algorithm tailored for underwater low-light and turbid environments based on the AquaVisNet model. Section 4 explores an image enhancement algorithm designed for underwater low-light and turbid conditions utilizing a serial-parallel fusion processing strategy. Section 5 elaborates on the construction of the experimental site and provides experimental verification of the robustness and localization accuracy of the proposed underwater visual SLAM system in low-light and turbid underwater settings. Section 6 concludes with a summary of the research presented in this paper.

2. Underwater visual SLAM system with adaptive image enhancement for underwater low-light and turbid environments

We present a novel monocular visual SLAM system called AIE-ORB-SLAM, which is specifically designed for low-light and turbid underwater environments. The overall architecture is visualized in Fig. 1. Grounded in the ORB-SLAM3 framework, the AIE-ORB-SLAM system consists of three concurrent threads (tracking, local underwater mapping, loop and underwater map merging) and incorporates a comprehensive underwater map management system.

2.1. Tracking thread

The tracking thread assumes the responsibility for computing the pose of the underwater camera and determining whether to generate new underwater keyframes. To address the challenges posed by the underwater low-light and turbid environment, the AIE-ORB-SLAM system proposed in this paper is designed with constraints specific to underwater environment recognition and adaptive underwater image enhancement in the visual odometry section. An underwater environment recognition algorithm based on the AquaVisNet model is designed to handle underwater environment recognition constraints. Additionally, an image enhancement algorithm for underwater low-light and turbid conditions employing a serial-parallel fusion processing strategy is designed to meet the adaptive underwater image enhancement constraints. By leveraging these two specific constraints, the AIE-ORB-SLAM system can extract and analyze underwater image features to determine the underwater operating environment and enhance images accordingly, resulting in maximally visualized underwater recovery images. After enhancing the original distorted underwater image, the feature points are matched to initialize, track, or recalibrate the current camera pose. Subsequently, the tracking thread determines whether the current frame qualifies as an underwater keyframe based on predefined decision criteria.

2.2. Local underwater mapping thread

The localized underwater mapping thread assumes a critical role in constructing, updating, and upholding localized underwater maps to ensure their consistency and real-time accessibility. This thread utilizes

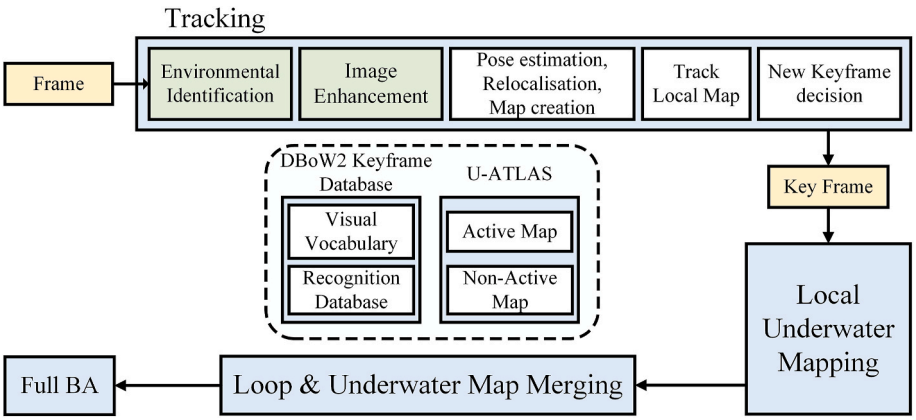

Fig. 1. Schematic of the AIE-ORB-SLAM system structure.

carefully chosen underwater keyframes to establish or refresh the underwater map, which includes essential relative pose information regarding the underwater map points and the underwater keyframes. When identical underwater map points are detected across multiple underwater keyframes, the thread consolidates these observations, thereby enhancing the consistency and precision of the underwater map. To maintain the scalability and dependability of the underwater map, redundant underwater keyframes are systematically removed.

2.3. Loop and underwater map merging thread

The loop and underwater map merging thread plays a pivotal role in loop detection, loop validation, closure operations, underwater map fusion, and the execution of global optimization. Its objective is to compare recently added underwater keyframes with all frames residing within the U-Atlas system. If similar frames are identified across different underwater maps, the two underwater maps are consolidated into a new active underwater map. In the absence of such similarity, a pose-graph optimization is executed to mitigate accumulated drift errors within the active map.

2.4. Multiple underwater map management system

U-Atlas is an underwater map management system that includes a collection of distinct underwater maps generated by AIE-ORB-SLAM. Within this system, the active map, utilized by the tracking thread for frame localization, is differentiated from the nonactive underwater maps. Additionally, the system establishes a unique DBoW2 identification database that includes all underwater maps. This database stores comprehensive information for identifying any underwater keyframe within any underwater map, facilitating tasks such as relocation, loop detection, and underwater map merging.

While ORB-SLAM3 (Campos et al., 2021) exhibits commendable performance when employed with a monocular camera in well-illuminated settings, its accuracy and resilience significantly decline in low-light and turbid underwater environments. This decline is primarily attributed to the deterioration in feature extraction and matching capabilities when processing underwater images in such challenging contexts. In scenarios where an insufficient number of matching ORB feature points are derived from the underwater surroundings, the pose estimation process encounters obstacles and may even result in initialization and tracking failures. Consequently, it is crucial to integrate a recognition algorithm customized for low-light and turbid underwater conditions based on the AquaVisNet model. Additionally, an image enhancement algorithm tailored for these underwater environments utilizing a serial-parallel fusion processing strategy should be included within the tracking thread.

By integrating underwater environment recognition and image enhancement into the image preprocessing stage, the AIE-ORB-SLAM system can identify the current underwater conditions and apply targeted enhancement techniques to restore degraded images in dynamic environments. This underwater environment recognition capability enables the system to adapt to dynamic changes in underwater conditions, while the image enhancement techniques specifically address the degradation of underwater image quality. This enhancement strengthens the robustness and precision of SLAM for robots operating under dynamic underwater conditions.

3. Recognition algorithm for underwater low-light and turbid environments based on the AquaVisNet model

To restore degraded underwater images, a recognition algorithm based on the AquaVisNet model designed for low-light and turbid underwater environments is proposed. The algorithm enhances image recovery efficiency in such underwater conditions by identifying the operational environment of the underwater robot.

3.1. AquaVisNet model structure

The classical convolutional neural network LeNet5 model has demonstrated the efficacy of using convolutional, pooling, and fully connected layer architectures for image classification tasks. In a similar vein, Altwaijry et al. (Altwaijry and Al-Turaiki, 2020) successfully utilized a convolutional neural network model with three convolutional layers, three pooling layers, and four fully connected layers to classify images into 29 categories. Inspired by these successes, a lightweight AquaVisNet model was developed in this study. The model, as illustrated in Fig. 2. And the configuration of each layer is shown in Table 1.

The AquaVisNet model has seven layers. Through two convolutional layers, the model extracts features such as color, texture, contrast, and shape from the images. Subsequently, two pooling layers are utilized to retain salient features, followed by a flattening layer and two fully connected layers to determine the image categories. The model also incorporates the ReLU activation function to enhance its ability to learn nonlinear features. It accepts underwater images of size 128 × 128 pixels with 3 channels. This particular resolution strikes a balance between reducing computational complexity while capturing crucial features for model training, such as underwater object color and contrast.

3.2. AquaVisNet model training process and results

We maneuver the ROV in a laboratory-built pool which replicates a marine environment to capture a dataset of images featuring underwater coral colonies in various environments. The AquaVisNet model is trained on a dataset comprising 8498 underwater coral images using a supervised learning approach. After removing low-quality images, 4000

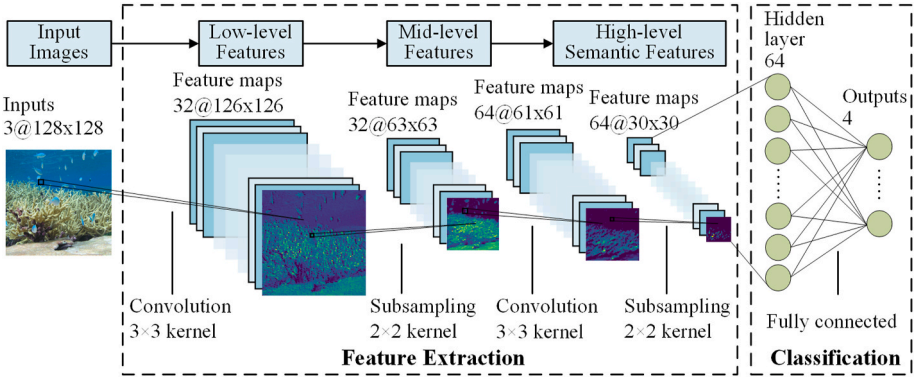

Fig. 2. AquaVisNet model structure.

Table 1
Configuration of AquaVisNet model layers.

Layer_name	Kernel_size	Kernel_num	Activation	Stride
Convolution_1	(3,3)	32	ReLU	1
Maxpool_1	(2,2)	/	/	2
Convolution _2	(3,3)	64	ReLU	1
Maxpool_2	(2,2)	/	/	2
Flatten	/	/	/	/
Fully Connected_1	64	/	ReLU	/
Fully Connected_2	4	/	Softmax	/

random samples were extracted to serve as the training set for the AquaVisNet model. Additionally, 1712 samples from the original dataset were designated as the validation set. Maintaining a consistent number of samples in each category in the training and validation sets was crucial for enabling the model to effectively learn the distinct features and patterns associated with each category. Exemplary images from both the training and validation sets are shown in Fig. 3.

The experimental hardware platform used in this study was configured as follows: the Win 10 operating system, Python 3.7, and an RTX1660. The initial learning rate for the network model is established at 0.001, and the cross-entropy loss function is applied. The training set comprises 4000 samples, while the validation set includes 1712 samples. To enhance the network model's performance, training consisted of 10 epochs, with a batch size of 32. Throughout the network training process, the accuracy and loss values for both the training and validation sets are recorded at each epoch.

The training process and the resulting results of the model are visualized in Fig. 4. To evaluate the model's performance, the cross-entropy loss function was employed, and model training utilized a stochastic gradient descent optimizer. After completing the training process, the AquaVisNet model achieved an accuracy of 97.23% for the training set and 96.54% for the validation set. And the training set attained a loss value of 0.15, while the validation set recorded a loss value of 0.17. Through precise fine-tuning, the model achieved an environment recognition accuracy of 99.58% under underwater low-light and turbid conditions.

4. Image enhancement algorithm for underwater low-light and turbid environments based on a serial-parallel fusion processing strategy

Underwater images often face adverse aquatic conditions that cause image degradation, such as blurring, reduced contrast, and color distortion (Zhang et al., 2022c), (Chen et al., 2025b). Conventional robots use directional lighting to capture images in low-light underwater environments, but these images may still have patches of low brightness and areas of light and dark patches. Such low-quality images can negatively impact the performance of the SLAM system. Hence, we present an image enhancement algorithm designed specifically for low-light underwater environments based on the CLAHE method. Additionally, an image enhancement algorithm is proposed for turbid underwater conditions based on the DCP method. To effectively utilize the synergy of these two image enhancement algorithms, a serial-parallel fusion strategy for image enhancement processing is introduced.

4.1. Image enhancement algorithm for underwater low-light environments based on CLAHE

In low-light underwater conditions, images suffer from insufficient lighting, resulting in regions of the image appearing excessively dim, thus affecting the performance of SLAM (Vargas et al., 2021), (Zhang et al., 2021). Fang et al. used the histogram equalization (HE) algorithm in the ORB-SLAM framework, which demonstrated enhanced robustness in harsh environments. However, HE is more sensitive to background noise (Fang et al., 2018). Yang et al. (Yang and Zhai, 2019) and Rahman et al. (2022) both employed the CLAHE algorithm in the ORB-SLAM framework, which effectively enhances SLAM performance in low-light and turbid underwater environments. Therefore, we propose an image enhancement algorithm for low-light underwater

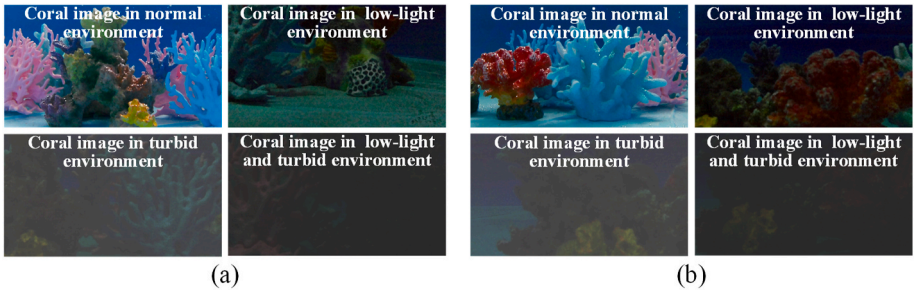

Fig. 3. Partial images of the training set and validation set. (a) Training set; (b) Validation set.

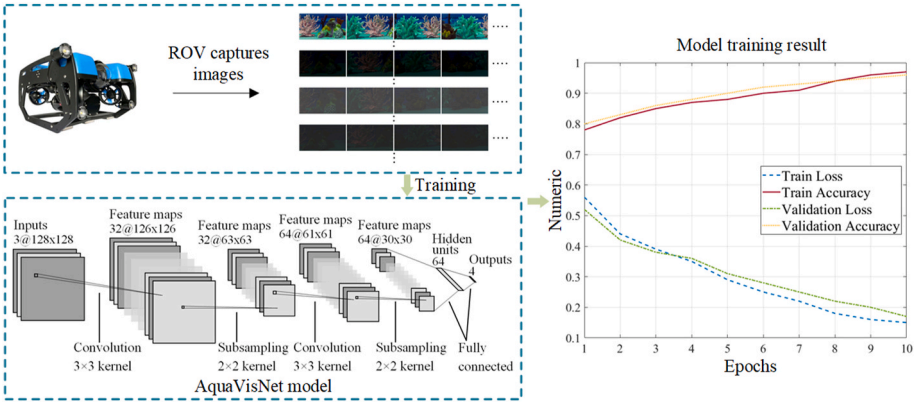

Fig. 4. Schematic of the AquaVisNet model training and training results.

environments called submerged CLAHE (SUB-CLAHE). SUB-CLAHE performs histogram equalization on all three color channels of an image within 20 ms and limits the extent of contrast enhancement during the equalization process to improve image quality and reveal more complex details.

The SUB-CLAHE algorithm primarily consists of the following steps, as illustrated in Fig. 5.

(1) Underwater low-light images are separated into three channels: B, G, and R. Each channel's image is segmented into localized image blocks of equal size, enabling independent processing of each local region.

(2) For each local image block, calculate its grayscale histogram $H(i)$, where i denotes the grayscales.

(3) The average number of pixels N_a assigned to each grayscale image is calculated as follows:

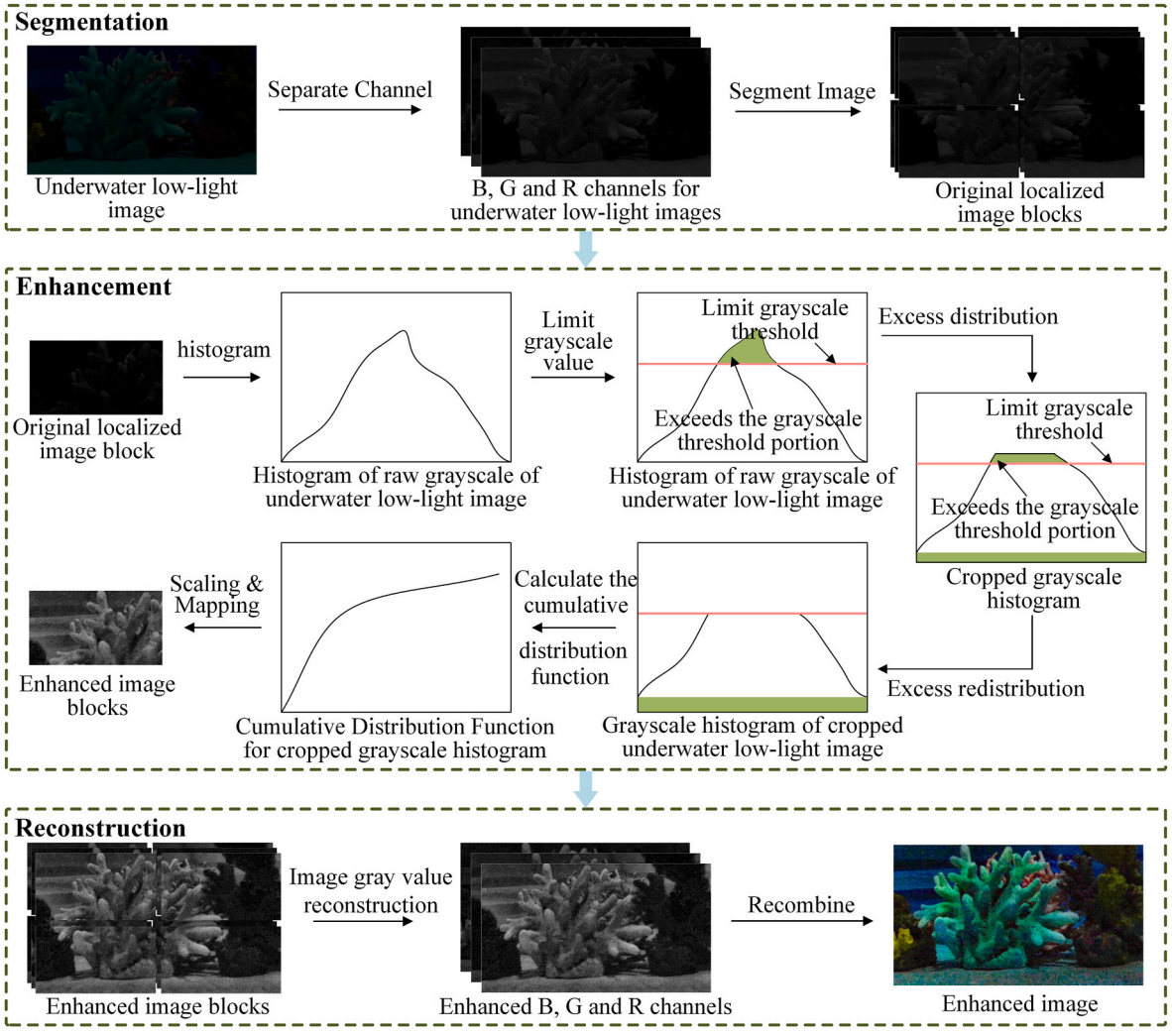

Fig. 5. Schematic of the SUB-CLAHE algorithm workflow.

$$N_a = \frac{(u_x \times u_y)}{L_g} \tag{1}$$

where u_x denotes the number of pixels in the horizontal direction, u_y denotes the number of pixels in the vertical direction, and L_g denotes the number of grayscales in the local image block.

(4) Histogram qualifying thresholds N_c are set based on the distribution of this histogram.

$$N_c = N_a + \left[\beta \times (u_x \times u_y - N_a)\right] \tag{2}$$

where β is the underwater low-light image grayscale histogram shear limiting factor.

(5) According to the qualifying threshold of each image block, a portion of the grayscale histogram that exceeds the threshold is clipped, and the clipped portion is uniformly distributed to each grayscale. Subsequently, following one iteration of allocation, the grayscale histogram of the local image block experiences an increment of one unit in height, surpassing the predefined qualifying threshold N_c, and the above operation is reiterated until the qualifying threshold is no longer exceeded.
(6) In line with the clipped histogram, histogram equalization is performed for each image block. This process aims to harmonize the distribution of pixel intensities within each image block, mitigating the adverse effects stemming from uneven illumination and enhancing the overall quality of the image.
(7) Considering the position of the image block, each pixel within the local image block is subjected to bilinear interpolation to reconstruct the pixel gray values. And the enhanced B, G, and R channel images are combined to create an enhanced color image. This step ensures seamless transitions between locally equalized regions, rendering the enhanced image visually cohesive and enriched with information.

4.2. Image enhancement algorithm for underwater turbid environments based on the dark channel prior principle

Both underwater turbid images and foggy images suffer from blurring due to the reflection and scattering of incident light by suspended particles within the medium (Thomas et al., 2021), (Muniraj and Dhandapani, 2021). Therefore, we model underwater turbid images and propose an image enhancement algorithm for underwater turbid environments based on the DCP, referred to as DCP underwater turbid images (DCP-UTI). The principle can be outlined as follows:

The underwater turbid image model is defined as follows:

$$U(x) = E(x)t(x) + B[1 - t(x)] \tag{3}$$

where $U(x)$ is the original underwater turbid image; $E(x)$ is the enhanced image; B is the background light component in the underwater environment; and $t(x)$ represents the underwater transmittance.

In the imaging model, normalization is achieved by dividing both sides by the background light value to the underwater environment for each channel, which can be obtained:

$$\frac{U^c(x)}{B^c} = t(x)\frac{E^c(x)}{B^c} + 1 - t(x) \tag{4}$$

Assuming that the underwater transmittance is a constant, we define it as $\tilde{t}(x)$ and minimize the operation twice for both sides of the above equation, which can be obtained:

$$\min_{y\in\Omega(x)}\left[\min_c \frac{U^c(y)}{B^c}\right] = \tilde{t}(x)\min_{y\in\Omega(x)}\left[\min_c \frac{E^c(y)}{B^c}\right] + 1 - \tilde{t}(x) \tag{5}$$

For an underwater clear image $E(x)$, the underwater dark channel tends to 0, i.e., $E^{dark}\to 0$ has:

$$E^{dark}(x) = \min_{y\in\Omega(x)}\left[\min_c E^c(y)\right] = 0 \tag{6}$$

Launch:

$$\min_{y\in\Omega(x)}\left[\min_c \frac{E^c(y)}{B^c}\right] = 0 \tag{7}$$

Substituting back into the original equation gives:

$$\tilde{t}(x) = 1 - \min_{y\in\Omega(x)}\left[\min_c \frac{U^c(y)}{B^c}\right] \tag{8}$$

To prevent the underwater image clarity from being too thorough, the turbidity limiting parameter $\omega = 0.95$ is introduced for water going down, which can be obtained:

$$\tilde{t}(x) = 1 - \omega\min_{y\in\Omega(x)}\left[\min_c \frac{U^c(y)}{B^c}\right] \tag{9}$$

The aforementioned derivation process presumes the availability of known background light values for underwater environments B. In practice, these values can be derived from the original underwater turbid image using the underwater dark channel map. The procedure unfolds as follows: Initially, the underwater dark channel map is computed, and the top 0.1% of pixels with the highest brightness are identified. Then, verify the chromatic consistency of these pixels. Subsequently, within the original underwater turbid image $U(x)$, the value corresponding to the position with the highest brightness point is extracted and employed as the background light value for underwater environments B.

Considering that a very small underwater transmittance t will lead to a large E-value, a threshold t_0 is set. Finally, the restoration formula for an underwater turbid image is organized as follows:

$$E(x) = \frac{U(x) - B}{\max[t(x), t_0]} + B \tag{10}$$

4.3. Experimental results and analysis of image enhancement algorithms

One randomly selected image from the dataset was processed using both the CLAHE and SUB-CLAHE image enhancement algorithms. The results are depicted in Fig. 6. Table 2 provides a quantitative comparison of the three images. Underwater color image quality evaluation (UCIQE) (Yang and Sowmya, 2015) and underwater image quality measure (UIQM) (Panetta et al., 2015) are metrics specifically designed for evaluating underwater image quality, effectively assessing features such as contrast, color saturation, and sharpness of underwater images. The experimental results reveal a significant decrease in the UCIQE and UIQM metrics of the image when the CLAHE image enhancement algorithm is applied due to the loss of color information. Specifically, compared with that of the original image, the UCIQE of the underwater image enhanced using the SUB-CLAHE algorithm improved by 28.48%, while the UIQM index increased by 28.93%. These improvements indicate enhanced image contrast and clearer texture details.

One image randomly selected from the dataset was processed using both the DCP image enhancement algorithm and the DCP-UTI image enhancement algorithm. The results are depicted in Fig. 7. Table 3 presents a quantitative comparison of the three images. Specifically, the UCIQE of the underwater image enhanced using the DCP-UTI algorithm improved by 31.68%, and the UIQM index increased by 32.56% compared to the original image. The UCIQE of the underwater image enhanced using the DCP-UTI algorithm improved by 14.93%, and the UIQM index increased by 22.43% compared to that of the underwater image enhanced using the DCP algorithm. These enhancements indicate a reduction in image turbidity, improved contrast, clearer texture details.

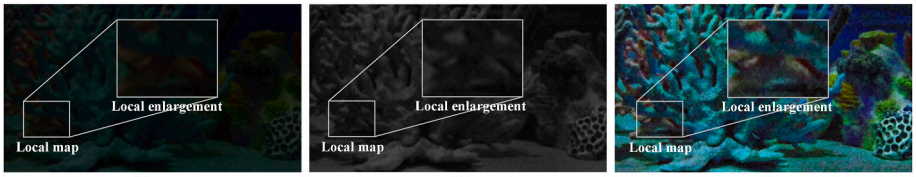

Fig. 6. Image enhancement results in low-light environments. (a) Original image; (b) Image enhanced by the CLAHE algorithm; (c) Image enhanced by the SUB-CLAHE algorithm.

Table 2
Comparison of reference-free quality evaluations of underwater low-light images.

Method	UCIQE	UIQM
Original underwater low-light image	0.4221	1.7651
CLAHE	0.2447	0.1764
SUB-CLAHE (ours)	**0.5423**	**2.2758**

4.4. Image enhancement processing strategy based on serial-parallel fusion

The underwater environment experiences real-time variations influenced by factors such as time, location, and depth. To enhance the robustness performance of underwater image visualization restoration, we propose an image enhancement processing strategy based on serial-parallel fusion, and the workflow is depicted in Fig. 8.

The ROV captures images of the current underwater environment and transmits them to the system. The system first performs environmental recognition to identify the characteristics of the current underwater environment. After recognition, the system uses average brightness and blur index as evaluation metrics for image brightness and turbidity. Among these, the average brightness metric is defined as the mean brightness value of all pixels in the image, incorporating a brightness scaling factor to measure the overall brightness level of the image; the blur index is determined using the underwater image sharpness measure (UISM) (Panetta et al., 2015).

The system relies on optical property sensing and underwater image quality assessment to select suitable image enhancement parameters and processing methods. When the system detects a low-light underwater environment, it calculates the average brightness metric of the image and adjusts the parameters of the SUB-CLAHE algorithm accordingly to optimize enhancement, improving image visibility and detail preservation. For low-light images with low average brightness, the system appropriately increases the qualifying thresholds of the three channels in the SUB-CLAHE algorithm to enhance more details and contrasts. The system can also increase the division of the image grid to handle local areas more finely. On the other hand, for low-light images with high average brightness, the qualifying thresholds of the three channels are appropriately reduced to balance detail enhancement and noise control. The system selects image grid divisions ranging from 8×8 to 16×16 to ensure balanced local and overall contrast. When the system detects a turbid underwater environment, it calculates the UISM metric of the image and adjusts the parameters of the DCP-UTI algorithm accordingly to optimize enhancement, improving image visibility and detail preservation. For turbid images with low UISM values, the system appropriately reduces the de-turbidity limiting parameter and increases the clarity parameter in the DCP-UTI algorithm to remove more turbidity and improve clarity. For turbid images with high UISM values, the system appropriately increases the de-turbidity limiting parameter and reduces the clarity parameter in the DCP-UTI algorithm to retain more image information and avoid excessive removal of turbidity. When the system detects a low-light and turbid underwater environment, it calculates the average brightness and UISM metrics of the image, then adjusts the parameters of the SUB-CLAHE and DCP-UTI algorithms accordingly to optimize enhancement, improving image visibility and detail preservation.

5. Experimental results and analysis

5.1. Experimental site construction

We have established an experimental system in a pool to replicate marine conditions, enabling the assessment of the algorithm proposed in this paper. Fig. 9 depicts the configuration of the experimental site, which consists of a pool, a Blue ROV2, and artificial coral colonies. The pool is 3.0 m long, 2.0 m wide, and 1.5 m high. The experimental scene for data collection with the ROV is shown in Fig. 10. During the experimental phase, the robot's movement is primarily recorded using a camera fixed on the top of the pool. This camera captures the robot's motion process in the X-Y plane, capturing its left-right and forward-backward motions. The resulting motion image sequence is then processed to obtain the ground truth by converting the trajectory in the pixel coordinate system to a real trajectory in the world coordinate system using the camera's intrinsic and extrinsic parameters and the scale factor. To simulate the conditions of marine coral colonies in a water-filled pool, various species of artificial corals are randomly arranged to create artificial coral colonies that closely resemble the operational environment of the ROV in the ocean. This experimental system can simulate key challenges encountered in marine

Table 3
Comparison of reference-free quality evaluations of underwater turbid images.

Method	UCIQE	UIQM
Original underwater turbid image	0.4384	1.9321
DCP	0.5023	2.0919
DCP-UTI (ours)	**0.5773**	**2.5612**

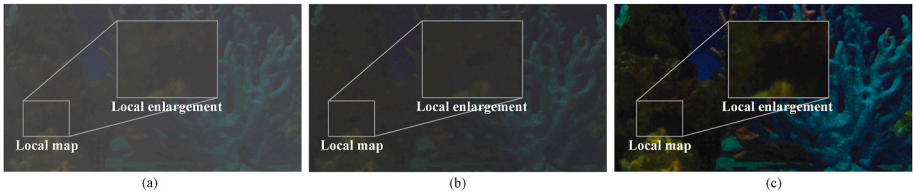

Fig. 7. Image enhancement results in turbid environments. (a) Original image; (b) Image enhanced by the DCP algorithm; (c) Image enhanced by the DCP-UTI algorithm.

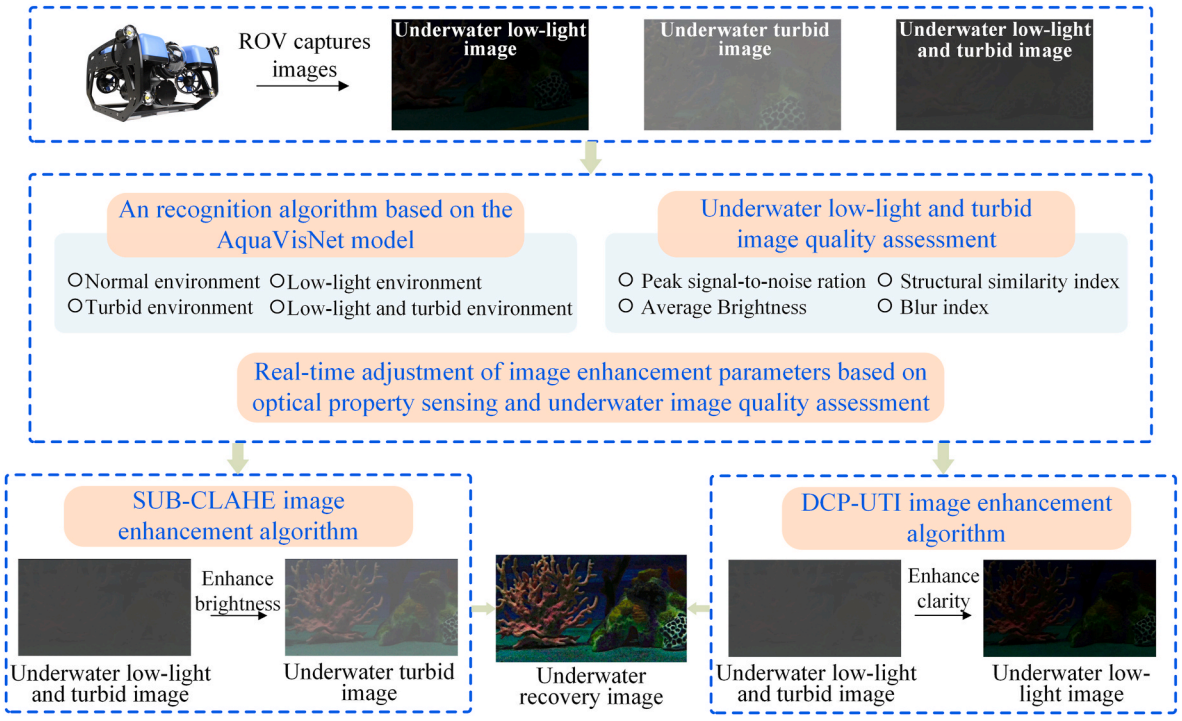

Fig. 8. Flowchart of the image enhancement processing strategy based on serial-parallel fusion.

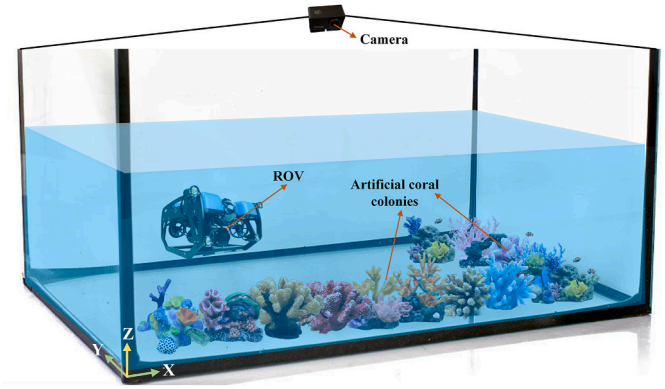

Fig. 9. Schematic of the experimental site.

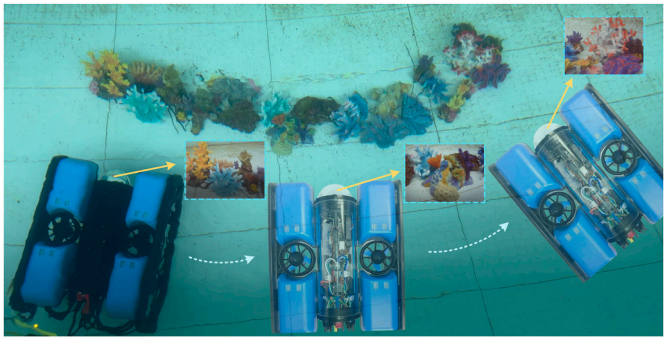

Fig. 10. Experimental scene for data collection with the ROV.

environments, such as decreasing environmental brightness and changes in water turbidity. By gradually adjusting variables such as underwater light intensity and turbidity in this controlled environment, we can effectively assess the performance of the underwater visual SLAM system in different conditions.

5.2. Camera calibration

A Blue ROV2 is used to conduct camera calibration experiments in a pool simulating a marine environment. The camera internal parameters K and the distortion correction coefficients k_1, k_2, p_1, p_2, and k_3 were obtained as follows:

$$K = \begin{bmatrix} f_x & 0 & c_x \\ 0 & f_y & c_y \\ 0 & 0 & 1 \end{bmatrix} = \begin{bmatrix} 615.370616 & 0.000000 & 317.848201 \\ 0.000000 & 614.814093 & 239.591827 \\ 0.000000 & 0.000000 & 1.000000 \end{bmatrix} \quad (11)$$

$$[k_1, k_2, p_1, p_2, k_3] = [-0.286117, 0.179157, -0.001363, 0.001407, 0.000000] \quad (12)$$

where f_x and f_y denote the focal length in the horizontal and vertical directions, respectively; c_x and c_y denote the coordinate positions of the camera's optical center in the image coordinate system; k_1, k_2, and k_3 are the radial distortion parameters; p_1 and p_2 are the tangential distortion parameters.

5.3. Underwater visual SLAM system effectiveness evaluation

To evaluate the effectiveness of the AIE-ORB-SLAM system, the ROV captures offline datasets of the underwater environment in the simulated marine environment pool under four conditions: normal, low light, turbidity, and both low light and turbidity, as shown in Fig. 11. Two distinct motion trajectories (I and II) are employed for data collection. We chose ORB-SLAM3, an open-source system that performs well in underwater environments, as a comparison benchmark for experimental evaluation. The same offline dataset is then fed into both the AIE-ORB-SLAM system and the ORB-SLAM3 system on an external computer to enable a comparative evaluation of the two SLAM systems in terms of robustness and localization accuracy. All the evaluations are based on the same offline dataset. To ensure the reliability of the experimental data, the reported results are the median values obtained from each

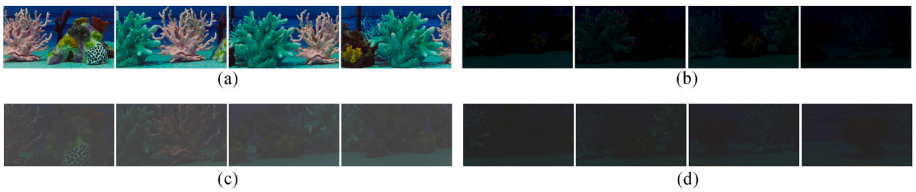

Fig. 11. Partial images of the dataset obtained from the experiment. (a) Normal environment; (b) Low-light environment; (c) Turbid environment; (d) Low-light and turbid environment.

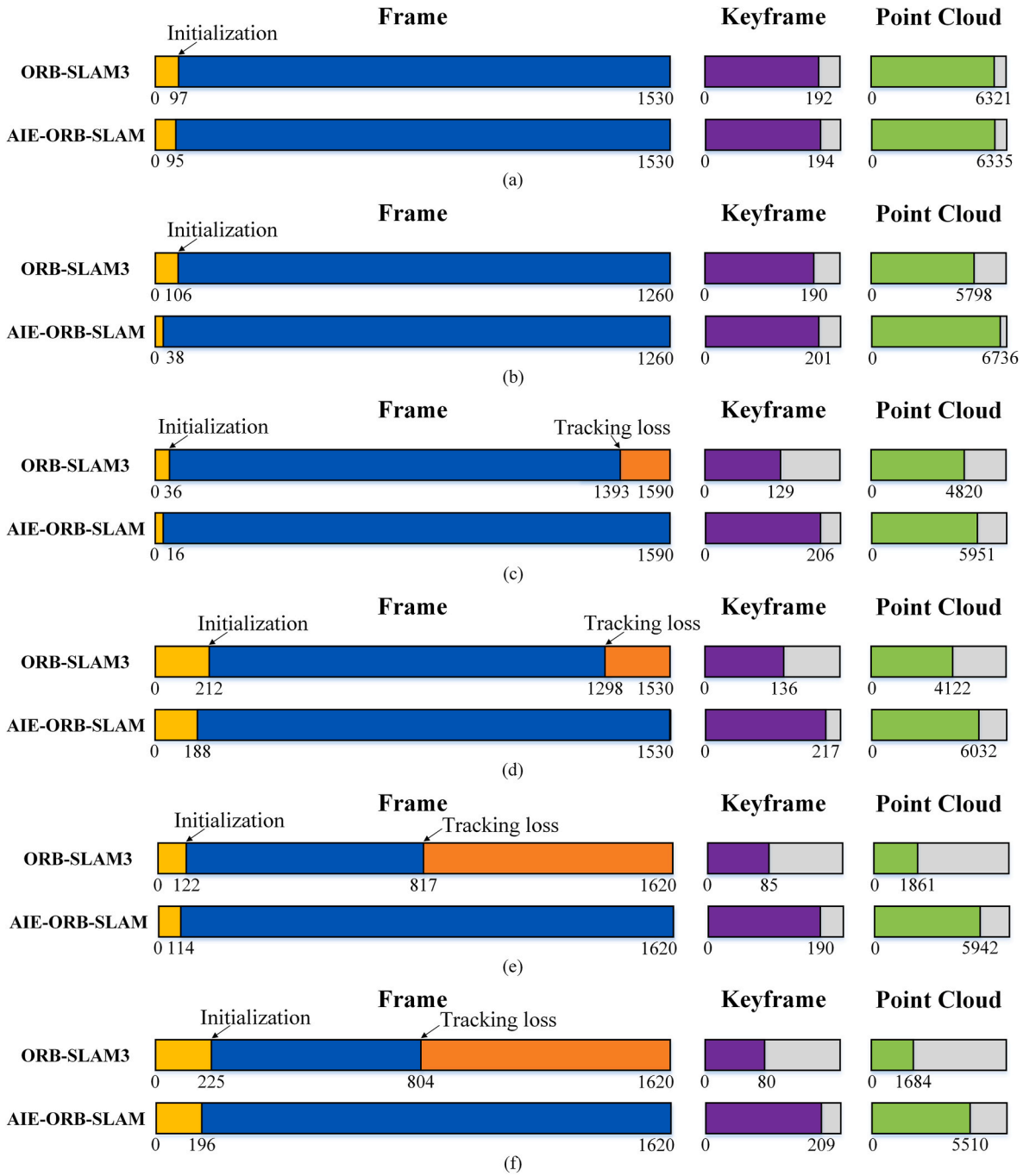

Fig. 12. SLAM operation result data for trajectory I. (a) Normal environment; (b) Low-light environment A; (c) Low-light environment B; (d) Low-light environment C; (e) Turbid environment; (f) Low-light and turbid environment.

SLAM system after running the identical dataset a total of 10 times.

5.3.1. Robustness evaluation

During the operation of the underwater visual SLAM system, various key parameters, such as initialization, tracking duration, keyframes, and point cloud data, were rigorously recorded. Specifically, initialization time refers to the duration required for the underwater visual SLAM system to complete initial map construction and camera pose estimation from startup, while tracking duration indicates the length of time the system can maintain stable tracking. Please refer to Figs. 12 and 13 for a detailed depiction of these parameters.

In the normal environment trajectory I dataset, both ORB-SLAM3 and AIE-ORB-SLAM achieved similar performances in terms of initialization, tracking loss, keyframes, and point clouds. However, in the low-light environment C trajectory I dataset, the AIE-ORB-SLAM system exhibited notable improvements. Compared to the ORB-SLAM3 system, the AIE-ORB-SLAM system achieved an 11.32% decrease in initialization time, a 23.57% increase in tracking duration, a 59.56% increase in the number of keyframes, and a 46.34% increase in the number of point clouds. When considering the turbid environment trajectory I dataset, the AIE-ORB-SLAM system demonstrated more improvements. Compared to the ORB-SLAM3 system, the AIE-ORB-SLAM system achieved a 6.56% decrease in initialization time, a 116.69% increase in tracking duration, a 123.53% increase in the number of keyframes, and a 219.29% increase in the number of point clouds. Finally, in the low-light and turbid environment trajectory I dataset, the

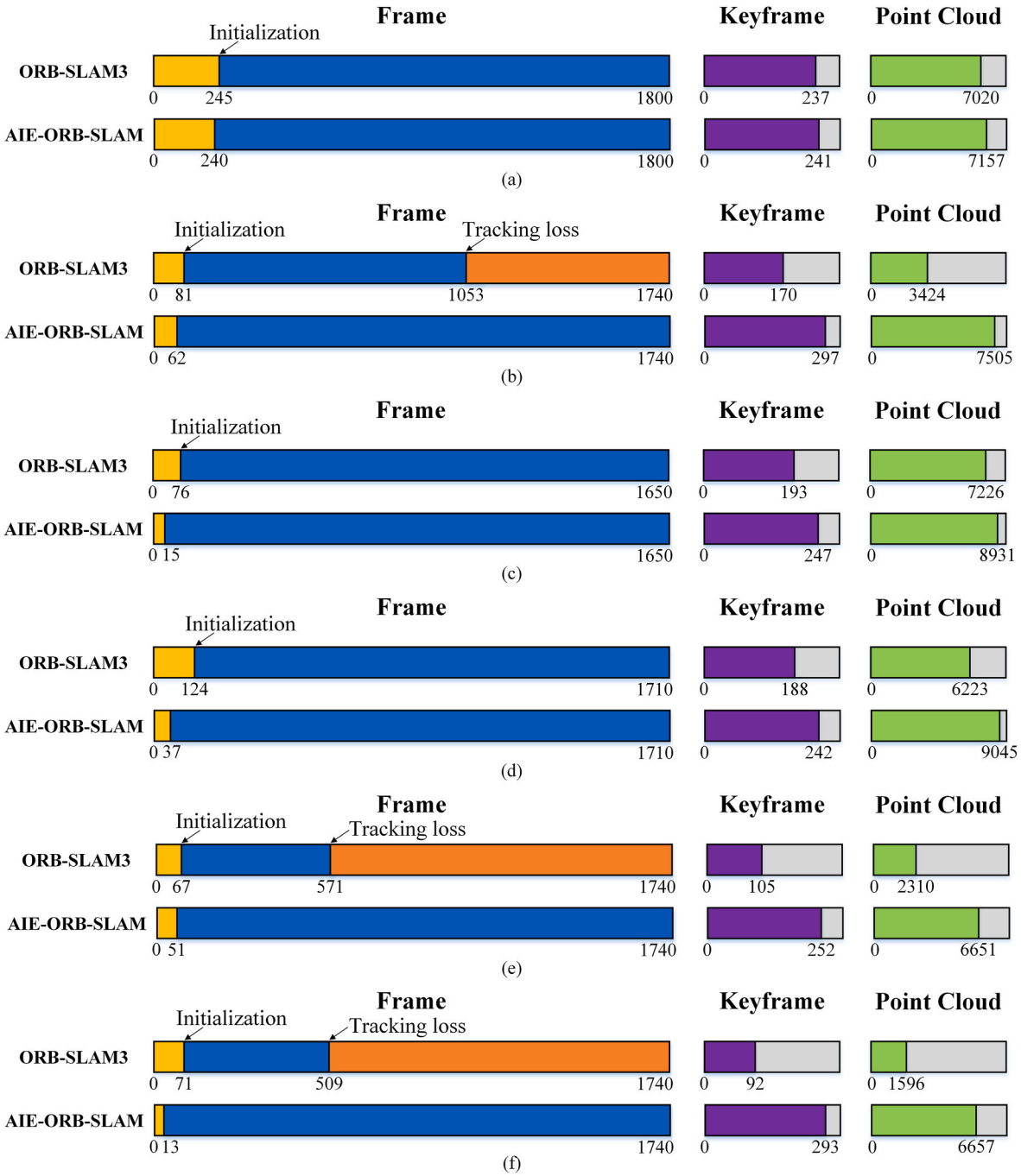

Fig. 13. SLAM operation result data for trajectory II. (a) Normal environment; (b) Low-light environment; (c) Turbid environment A; (d) Turbid environment B; (e) Turbid environment C; (f) Low-light and turbid environment.

AIE-ORB-SLAM system showed remarkable enhancements. Compared to the ORB-SLAM3 system, the AIE-ORB-SLAM system achieved a 12.89% decrease in initialization time, a 145.94% increase in tracking duration, a 161.25% increase in the number of keyframes, and a 227.20% increase in the number of point clouds.

Using the low-light environment trajectory I dataset, we examine three datasets with varying light intensities and quantitatively assessed their light intensities using the average brightness metric. In the low-light environment A trajectory I dataset, which has an average brightness of 1.1119, the AIE-ORB-SLAM system presented notable improvements over the ORB-SLAM3 system. Specifically, the AIE-ORB-SLAM system achieved a 64.15% decrease in initialization time, a 5.89% increase in tracking duration, a 5.79% increase in the number of keyframes, and a 16.18% increase in the number of point clouds. Similarly, in the low-light B trajectory I dataset, with an average brightness of 0.4077, the AIE-ORB-SLAM system exhibited substantial improvements over the ORB-SLAM3 system. The improvements included a 55.56% decrease in initialization time, a 15.99% increase in tracking duration, a 59.69% increase in the number of keyframes, and a 23.46% increase in the number of point clouds. Finally, in the low-light environment C trajectory I dataset, which has an average brightness of 0.1966, the AIE-ORB-SLAM system demonstrated enhancements over the ORB-SLAM3 system. Specifically, the AIE-ORB-SLAM system achieved an 11.32% decrease in initialization time, a 23.57% increase in tracking duration, a 59.56% increase in the number of keyframes, and a 46.34% increase in the number of point clouds.

In the normal environment trajectory II dataset, both ORB-SLAM3 and AIE-ORB-SLAM demonstrated similar performances in terms of initialization, tracking loss, keyframes, and point clouds. However, in the low-light environment trajectory II dataset, the AIE-ORB-SLAM system showed enhancements of 23.46% in initialization time, 72.63% in tracking duration, 74.71% in the number of keyframes, and 119.19% in the number of point clouds compared to the ORB-SLAM3 system. Similarly, in the turbid environment C trajectory II dataset, the AIE-ORB-SLAM system presented improvements of 23.88% in initialization time, 235.12% in tracking duration, 140.00% in the number of keyframes, and 187.92% in the number of point clouds compared to the ORB-SLAM3 system. Finally, in the low-light and turbid environment trajectory II dataset, the AIE-ORB-SLAM system exhibited substantial improvements—81.69% in initialization time, 294.29% in tracking duration, 218.48% in the number of keyframes, and 317.11% in the number of point clouds—when compared to the ORB-SLAM3 system.

Moreover, for the turbid environment trajectory II dataset, we compare three datasets with different turbidity levels and quantitatively assessed their turbidity using the UISM metric. In the turbid environment A trajectory II dataset with a UISM of 0.7620, the AIE-ORB-SLAM system yielded improvements of 80.26% in initialization time, 3.88% in tracking duration, 27.98% in the number of keyframes, and 23.60% in the number of point clouds relative to the ORB-SLAM3 system. Similarly, in the turbid environment B trajectory II dataset with a UISM of 0.6052, the AIE-ORB-SLAM system exhibited substantial improvements—70.16% in initialization time, 5.49% in tracking duration, 28.72% in the number of keyframes, and 45.35% in the number of point clouds—when compared to the ORB-SLAM3 system. In the turbid environment trajectory C II dataset with a UISM of 0.4910, the AIE-ORB-SLAM system presented enhancements of 23.88% in initialization time, 235.12% in tracking duration, 140.00% in the number of keyframes, and 187.92% in the number of point clouds compared to the ORB-SLAM3 system.

In the underwater visual SLAM system, faster initialization, longer tracking duration, and higher numbers of keyframes and point clouds indicate that the system can operate stably for longer periods, more comprehensively extract and represent underwater environmental information, generate more detailed and higher-quality maps, and ultimately improve the system's robustness. Therefore, based on the experimental findings, it can be inferred that the AIE-ORB-SLAM system outperforms the ORB-SLAM3 system in underwater low-light and turbid environments, demonstrating its superior robustness.

5.3.2. *Precision evaluation*

We utilize the absolute trajectory error (ATE) metric to evaluate the accuracy of underwater visual SLAM systems (Zhang and Scaramuzza, 2018). Figs. 14 and 15 display the trajectories estimated by ORB-SLAM3, AIE-ORB-SLAM, and the ground truth trajectories. To enhance clarity, time frames for the beginning and end of the trajectories have been added to the figures. Notably, in underwater low-light and turbid environments, the estimated trajectories produced by the ORB-SLAM3 system tend to interrupt. Conversely, the estimated trajectories of the AIE-ORB-SLAM system remain stable and maintain close proximity to the actual trajectories.

To further evaluate the accuracy of the AIE-ORB-SLAM model, we compared the ATEs of the estimated trajectories and the actual trajectories for both the ORB-SLAM3 and AIE-ORB-SLAM systems. The results can be found in Tables 4 and 5. In the trajectory I dataset, the AIE-ORB-SLAM system demonstrates significant improvements in localization accuracy compared to the ORB-SLAM3 system. Specifically, there are enhancements of 50.17% in normal environments, 54.13% in low-light environments A, 77.43% in low-light environments B, 84.34% in low-light environments C, 20.29% in turbid environments, and 35.83% in low-light and turbid environments. For the trajectory II dataset, the AIE-ORB-SLAM system also outperforms the ORB-SLAM3 system, with improvements of 26.58% in normal environments, 90.04% in low-light environments, 64.64% in turbid environments A, 67.07% in turbid environments B, 75.61% in turbid environments C, and 66.81% in low-light and turbid environments. These results demonstrate the consistent superiority of the AIE-ORB-SLAM system in terms of localization accuracy, particularly in low-light and turbid underwater environments, compared to the ORB-SLAM3.

The experimental results indicate that the AIE-ORB-SLAM system, as proposed in this paper, exhibits remarkable robustness and achieves higher localization accuracy in underwater low-light and turbid environments than does the ORB-SLAM3 system. Furthermore, this approach enables precise underwater robot localization and map construction, even under these challenging underwater conditions.

6. Conclusion

This paper effectively addresses the issue of performance degradation in underwater visual SLAM when operating in low-light and turbid underwater environments. We present a two-pronged solution: first, a recognition algorithm based on the AquaVisNet model is proposed, facilitating real-time recognition of the underwater environment. Second, an image enhancement algorithm employing a serial-parallel fusion processing strategy is introduced to adaptively restore degraded underwater images, optimizing visibility and quality.

The culmination of these innovations is the AIE-ORB-SLAM system, an integration of recognition and image enhancement algorithms. An experimental evaluation was conducted on various underwater environment datasets to demonstrate the superiority of the AIE-ORB-SLAM system over the ORB-SLAM3 system. The evaluation showed the system's advantages, such as shorter initialization time, extended tracking duration, enhanced mapping capabilities, and superior localization accuracy, even under low-light and turbid underwater conditions. The AIE-ORB-SLAM system excels at accurately identifying the current underwater environment and performing adaptive image enhancement, enabling precise and reliable SLAM for underwater robots, even in dynamic underwater environments.

Future research endeavors will refine the underwater environment recognition model and expand the image enhancement algorithm. Additionally, a high-performance real-time motion capture device will be deployed on the robot to investigate the performance of the AIE-ORB-SLAM system in three-dimensional motion trajectories. Efforts will also

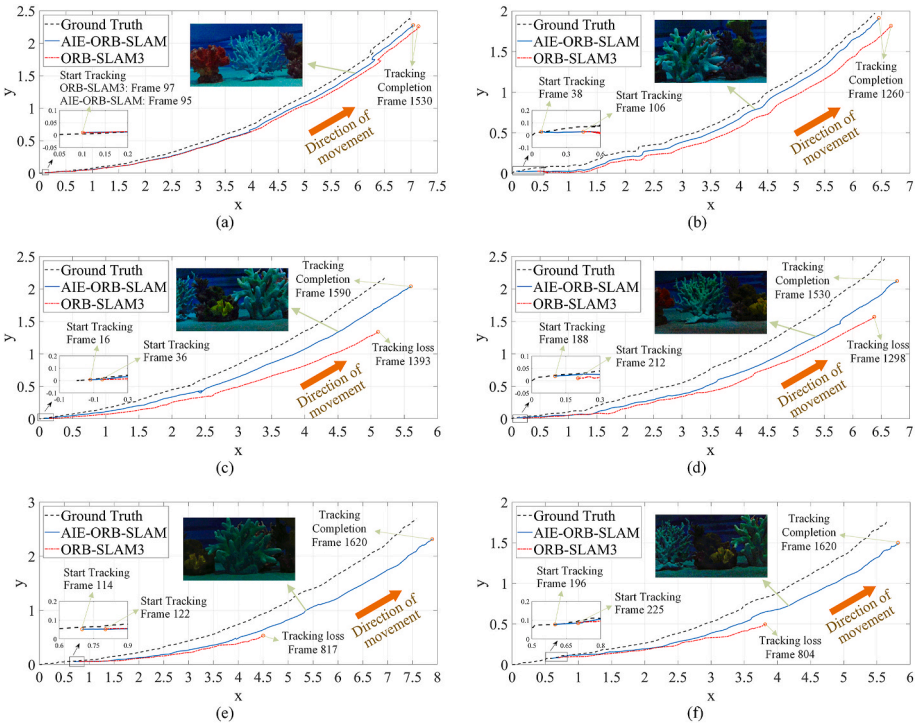

Fig. 14. ORB-SLAM3 and AIE-ORB-SLAM estimation trajectory plots for the trajectory I dataset. (a) Normal environment trajectory plot; (b) Low-light environment A trajectory plot; (c) Low-light environment B trajectory plot; (d) Low-light environment C trajectory plot; (e) Turbid environment trajectory plot; (f) Low-light and turbid environment trajectory plot.

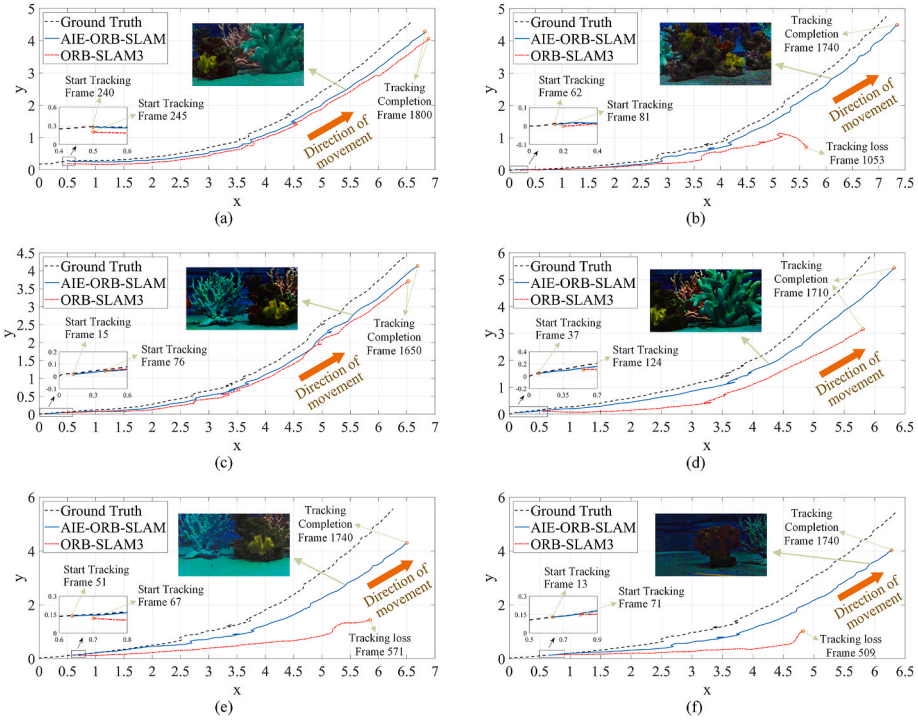

Fig. 15. ORB-SLAM3 and AIE-ORB-SLAM estimation trajectory plots for the trajectory II dataset. (a) Normal environment trajectory plot; (b) Low-light environment trajectory plot; (c) Turbid environment A trajectory plot; (d) Turbid environment B trajectory plot; (e) Turbid environment C trajectory plot; (f) Low-light and turbid environment trajectory plot.

Table 4
Mean ATE and RMS ATE from the operation of the underwater visual SLAM system on trajectory dataset I.

Type	ORB-SLAM3		AIE-ORB-SLAM (ours)	
	Mean ATE	RMS ATE	Mean ATE	RMS ATE
Normal Environment (Average Brightness: 2.0026)	0.2097	0.2176	**0.1045**	**0.1055**
Low-light Environment A (Average Brightness: 1.1119)	0.5095	0.5473	**0.2337**	**0.2426**
Low-light Environment B (Average Brightness: 0.4077)	0.9906	1.0721	**0.2236**	**0.2620**
Low-light Environment C (Average Brightness: 0.1966)	1.4205	1.5887	**0.2224**	**0.2413**
Turbid Environment	1.2199	1.3048	**0.9724**	**0.9985**
Low-light and Turbid Environment	1.2188	1.3421	**0.7821**	**0.8051**

Table 5
Mean ATE and RMS ATE from the operation of the underwater visual SLAM system on trajectory dataset II.

Type	ORB-SLAM3		AIE-ORB-SLAM (ours)	
	Mean ATE	RMS ATE	Mean ATE	RMS ATE
Normal Environment (UISM: 0.9667)	0.4071	0.4246	**0.2989**	**0.3115**
Low-light Environment	2.3116	2.8897	**0.2302**	**0.2378**
Turbid Environment A (UISM: 0.7620)	0.9344	1.0716	**0.3304**	**0.3464**
Turbid Environment B (UISM: 0.6052)	0.9339	0.9794	**0.3075**	**0.3275**
Turbid Environment C (UISM: 0.4910)	2.9058	3.0879	**0.7087**	**0.7467**
Low-light and Turbid Environment	1.6836	1.7230	**0.5588**	**0.5890**

be directed toward improving the computational efficiency and overall performance of the AIE-ORB-SLAM system. Validation of its reliability and robustness in authentic marine environments will be carried out through the application of the system to the ecological detection of coral colonies in marine environments.

CRediT authorship contribution statement

Gang Chen: Writing – review & editing, Writing – original draft, Visualization, Validation, Supervision, Software, Resources, Project administration, Methodology, Investigation, Funding acquisition, Conceptualization. **Guoqiang Du:** Writing – review & editing, Writing – original draft, Visualization, Validation, Software, Methodology, Investigation, Formal analysis, Data curation, Conceptualization. **Chenguang Yang:** Writing – review & editing, Supervision, Resources, Project administration, Methodology, Conceptualization. **Yidong Xu:** Supervision, Project administration, Methodology, Conceptualization. **Chuanyu Wu:** Supervision, Resources, Project administration, Conceptualization. **Huosheng Hu:** Writing – review & editing, Supervision, Resources. **Fei Dong:** Supervision, Resources. **Jinfeng Zeng:** Supervision, Resources.

Declaration of competing interest

The authors declare that they have no known competing financial interests or personal relationships that could have appeared to influence the work reported in this paper.

Acknowledgements

This work is financially supported by National Natural Science Foundation of China (Nos. 52275037, 51875528, and 41506116), Zhejiang Provincial Natural Science Foundation of China (No. LR24E050002), the Key Research and Development Project of Zhejiang Province (Nos. 2023C03015 and 2024C01257), the Emergency Management Research and Development Project of Zhejiang Province (No. 2024YJ026), the Key Research and Development Project of Ningxia Hui Autonomous Region (No. 2023BDE03002), and the Fundamental Research Funds of Zhejiang Sci-Tech University (No. 24242088-Y).

References

Altwaijry, N., Al-Turaiki, I., 2020. Arabic handwriting recognition system using convolutional neural network. Neural Comput. Appl. 33 (7), 2249–2261. https://doi.org/10.1007/s00521-020-05070-8.

Barros, A.M., Michel, M., Moline, Y., Corre, G., Carrel, F., 2022. A comprehensive survey of visual slam algorithms. Robot 11 (1), 24. https://doi.org/10.3390/robotics11010024.

Campos, C., Elvira, R., Rodríguez, J.J.G., Montiel, J.M.M., Tardós, J.D., 2021. Orb-slam3: an accurate open-source library for visual, visual–inertial, and multimap slam. IEEE Trans. Robot. 37 (6), 1874–1890. https://doi.org/10.1109/TRO.2021.3075644.

Chen, G., et al., 2023. Design and control of a novel bionic mantis shrimp robot. IEEE ASME Trans. Mechatron. 28 (6), 3376–3385. https://doi.org/10.1109/TMECH.2023.3266778.

Chen, G., et al., 2024. Target tracking control of a bionic mantis shrimp robot with closed-loop central pattern generators. Ocean Eng 297, 116963. https://doi.org/10.1016/j.oceaneng.2024.116963.

Chen, G., et al., 2025a. Motion stability analysis of beaver-like robot. Proc. Inst. Mech. Eng., Part M: J. Eng. Maritime Environ. https://doi.org/10.1177/14750902241311670.

Chen, G., et al., 2025b. Multi-performance index reinforcement learning training of beaver-like robot. Meas. Sci. Technol. 36 (3), 036204. https://doi.org/10.1088/1361-6501/adac01.

Cheng, C., Sha, Q., He, B., Li, G., 2021. Path planning and obstacle avoidance for AUV: a review. Ocean Eng. 235, 109355. https://doi.org/10.1016/j.oceaneng.2021.109355.

Fang, Y., et al., 2018. HE-SLAM: a stereo SLAM system based on histogram equalization and ORB features. Proc. Chin. Autom. Congr., Xi'an, China 4272–4276. https://doi.org/10.1109/CAC.2018.8623424.

Guo, Y., Li, H., Zhuang, P., 2020. Underwater image enhancement using a multiscale dense generative adversarial network. IEEE J. Ocean. Eng. 45 (3), 862–870. https://doi.org/10.1109/JOE.2019.2911447.

Hess, W., Kohler, D., Rapp, H., Andor, D., 2016. Real-time loop closure in 2D LIDAR SLAM. In: IEEE Int. Conf. Robot. Automat., Stockholm, Sweden, pp. 1271–1278. https://doi.org/10.1109/ICRA.2016.7487258.

Hidalgo, F., Kahlefendt, C., Bräunl, T., 2018. Monocular orb-slam application in underwater scenarios. In: OCEANS-MTS/IEEE Kobe Techno-Oceans. Kobe, Japan, pp. 1–4. https://doi.org/10.1109/OCEANSKOBE.2018.8559435.

Hodne, L.M., et al., 2022. Detecting and suppressing marine snow for underwater visual slam. In: Proc. IEEE/CVF Conf. Comput. Vis. Pattern Recog., New Orleans, USA, pp. 5101–5109.

Hu, C., Zhu, S., Liang, Y., Mu, Z., Song, W., 2021. Visual-pressure fusion for underwater robot localization with online initialization. IEEE Rob. Autom. Lett. 6 (4), 8426–8433. https://doi.org/10.1109/LRA.2021.3108584.

Huang, H., Lin, W.Y., Liu, S., Zhang, D., Yeung, S.K., 2020. Dual-slam: a framework for robust single camera navigation. In: IEEE/RSJ Int. Conf. Intell. Robots Syst. Las Vegas, USA, pp. 4942–4949. https://doi.org/10.1109/IROS45743.2020.9341513.

Jang, H., Yoon, S., Kim, A., 2021. Multi-session underwater pose-graph slam using inter-session opti-acoustic two-view factor. In: IEEE Int. Conf. Robot. Automat. Xi'an, China, pp. 11668–11674. https://doi.org/10.1109/ICRA48506.2021.9561161.

Joshi, B., et al., 2019. Experimental comparison of open source visual-inertial-based state estimation algorithms in the underwater domain. In: IEEE/RSJ Int. Conf. Intell. Robots Syst., pp. 7227–7233. https://doi.org/10.1109/IROS40897.2019.8968049. Macau, China.

Li, C., Anwar, S., Porikli, F., 2020. Underwater scene prior inspired deep underwater image and video enhancement. Pattern Recogn. 98 (107038). https://doi.org/10.1016/j.patcog.2019.107038.

Liu, Y., et al., 2023. An improved image enhancement method for underwater robot SLAM. In: IEECE Int. Conf. Mechatron. Automat., Harbin, China, pp. 2366–2371. https://doi.org/10.1109/ICMA57826.2023.10215743.

Mattern, J., et al., 2021. Underwater navigation using 3D vision, edge processing, and autonomy. In: OCEANS, San Diego, USA, pp. 1–6. https://doi.org/10.23919/OCEANS44145.2021.9705880.

Muniraj, M., Dhandapani, V., 2021. Underwater image enhancement by combining color constancy and dehazing based on depth estimation. Neurocomputing 460, 211–230. https://doi.org/10.1016/j.neucom.2021.07.003.

Panetta, K., Gao, C., Agaian, S., 2015. Human-visual-system-inspired underwater image quality measures. IEEE J. Ocean. Eng. 41 (3, 541–551. https://doi.org/10.1109/JOE.2015.2469915.

Rahman, S., Li, A.Q., Rekleitis, I., 2022. SVIn2: a multi-sensor fusion-based underwater SLAM system. Int. J. Robot Res. 41 (11/12), 1022–1042. https://doi.org/10.1177/02783649221110259.

Thomas, R., et al., 2021. Dehazing underwater images using encoder decoder based generic model-agnostic convolutional neural network. Int. Symp. Ocean Tech. (SYMPOL), Kochi, India 1–4. https://doi.org/10.1109/SYMPOL53555.2021.9689441.

Vargas, E., et al., 2021. Robust underwater visual SLAM fusing acoustic sensing. In: IEEE Int. Conf. Robot. Automat. Xi'an, China, pp. 2140–2146. https://doi.org/10.1109/ICRA48506.2021.9561537.

Wang, W., et al., 2023. Real-time dense 3d mapping of underwater environments. In: IEEE Int. Conf. Robot. Automat., London, UK, pp. 5184–5191. https://doi.org/10.1109/ICRA48891.2023.10160266.

Xin, Z., Wang, Z., Yu, Z., Zheng, B., 2023. ULL-SLAM: underwater low-light enhancement for the front-end of visual SLAM. Front. Mar. Sci. 10, 1133881. https://doi.org/10.3389/fmars.2023.1133881.

Xu, S., et al., 2021. Underwater visual acoustic SLAM with extrinsic calibration. In: IEEE/RSJ Int. Conf. Intell. Robots Syst., Prague, Czech Republic, pp. 7647–7652. https://doi.org/10.1109/IROS51168.2021.9636258.

Yan, L., et al., 2024. A dual-stage coverage path planning method for bathymetric survey using an AUV in graph-based SLAM framework considering positioning uncertainty. Ocean Eng 312, 109355. https://doi.org/10.1016/j.oceaneng.2024.119252.

Yang, M., Sowmya, A., 2015. An underwater color image quality evaluation metric. IEEE Trans. Image Process. 24 (12, 6062–6071. https://doi.org/10.1109/TIP.2015.2491020.

Yang, W., Zhai, X., 2019. Contrast limited adaptive histogram equalization for an advanced stereo visual slam system. In: Proc. Int. Conf. Cyber-Enabled Distrib. Comput. Knowl. Discov., Guilin, China, pp. 131–134. https://doi.org/10.1109/CyberC.2019.00030.

Zhang, Z., Scaramuzza, D., 2018. A tutorial on quantitative trajectory evaluation for visual (-inertial) odometry. In: IEEE/RSJ Int. Conf. Intell. Robots Syst., Madrid, Spain, pp. 7244–7251. https://doi.org/10.1109/IROS.2018.8593941.

Zhang, W., Dong, L., Zhang, T., Xu, W., 2021. Enhancing underwater image via color correction and bi-interval contrast enhancement. Signal Process. Image Commun. 90, 116030. https://doi.org/10.1016/j.image.2020.116030.

Zhang, S., et al., 2022a. Visual SLAM for underwater vehicles: a survey. Comput. Sci. Rev. 46, 100510. https://doi.org/10.1016/j.cosrev.2022.100510.

Zhang, W., et al., 2022b. Underwater image enhancement via minimal color loss and locally adaptive contrast enhancement. IEEE Trans. Image Process. 31, 3997–4010. https://doi.org/10.1109/TIP.2022.3177129.

Zhang, W., Wang, Y., Li, C., 2022c. Underwater image enhancement by attenuated color channel correction and detail preserved contrast enhancement. IEEE J. Ocean. Eng. 47 (3), 718–735. https://doi.org/10.1109/JOE.2022.3140563.

Zheng, Z., Xin, Z., Yu, Z., Yeung, S.-K., 2023. Real-time GAN-based image enhancement for robust underwater monocular SLAM. Front. Mar. Sci. 10, 1161399. https://doi.org/10.3389/fmars.2023.1161399.